ExoMol line lists – LVIII. High-temperature molecular line list of carbonyl sulphide (OCS)

Alec Owens*, Sergei N. Yurchenko and Jonathan Tennyson

Department of Physics and Astronomy, University College London, Gower Street, WC1E 6BT London, UK

Accepted XXXX. Received XXXX; in original form XXXX

ABSTRACT

A new molecular line list covering wavelengths $\lambda > 1$ μm (the 0 – 10 000 cm^{-1} range) for the main isotopologue of carbonyl sulphide ^{16}O^{12}C^{32}S is presented. The OCS line list, named OYT8, contains almost 2.5 billion transitions between 2.4 million rotation-vibration energy levels with the total angular momentum up to $J = 223$. It is suitable for high-temperature environments up to $T = 2000$ K. Line list calculations were performed with the variational nuclear motion code TROVE in conjunction with a highly accurate, empirically-refined potential energy surface and a newly computed *ab initio* dipole moment surface of OCS. The OYT8 line list is adapted for high-resolution applications by replacing computed energy levels with empirically-derived values of OCS where available. Comparisons of the OYT8 line list with other OCS line lists and spectra yields excellent agreement for both strong and weak spectroscopic bands. The increased coverage of the OYT8 line list and the many new spectral features that are available will greatly facilitate the future observation of OCS on exoplanets. Carbonyl sulphide joins a growing number of sulphur-bearing molecules available from the ExoMol database. The OYT8 line list along with the associated temperature- and pressure-dependent molecular opacities can be downloaded from www.exomol.com and the CDS astronomical database.

Key words: molecular data – opacity – planets and satellites: atmospheres – stars: atmospheres – ISM: molecules.

1 INTRODUCTION

Carbonyl sulphide (main isotopologue ^{16}O^{12}C^{32}S) is a prominent molecule in terrestrial and astronomical environments. On Earth, OCS is one of the most widespread sulphur-containing species in the atmosphere, produced by a variety of natural and anthropogenic sources (Lee & Brimblecombe 2016) and possessing a long atmospheric lifetime (Khalil & Rasmussen 1984). Surprisingly, its role in the prebiotic formation of biomolecules has been investigated, challenging conventional assumptions about prebiotic chemistry on Earth (Leman et al. 2004). Astronomically, it has been observed in many settings such as the interstellar medium (Jefferts et al. 1971), comets (Woodney et al. 1997), nearby galaxies (Mauersberger et al. 1995), the atmosphere of Venus (Bézard et al. 1990), and in the atmosphere of Jupiter after collision with fragments from the comet Shoemaker–Levy 9 (Lellouch et al. 1995). Recently, the James Webb Space Telescope (JWST) Early Release Science programme Ice Age has been documenting the rich composition of dense molecular cloud ices and identified weak ice absorption features of OCS amongst a select number of other molecules (McClure et al. 2023).

Major studies of extrasolar planets, known as exoplanets, are actively searching for spectroscopic signatures of OCS, e.g. in JWST spectra of the gas giant WASP-39b (Tsai et al. 2023; Alderson et al. 2023). The infrared spectrum of OCS has been extensively studied in the laboratory, see the review by Xu & Tennyson (2023). However, there is currently no published, infrared OCS molecular line list suitable for the high-temperature environments commonly found on exoplanets, hindering its potential detection. Only room-temperature OCS line list data with incomplete coverage is available from the HITRAN

* The corresponding author: alec.owens.13@ucl.ac.uk

© The Author(s) 2024. Published by Oxford University Press on behalf of Royal Astronomical Society. This is an Open Access article distributed under the terms of the Creative Commons Attribution License (http://creativecommons.org/licenses/by/4.0/), which permits unrestricted reuse, distribution, and reproduction in any medium, provided the original work is properly cited.

ORIGINAL UNEDITED MANUSCRIPT

Downloaded from https://academic.oup.com/mnras/advance-article/doi/10.1093/mnras/stae1110/7657811 by guest on 28 April 2024

(HIgh-resolution TRANsmission) molecular spectroscopic database (Gordon et al. 2022), and absorption cross-sections from the Pacific Northwest National Laboratory (PNNL) spectral library (Sharpe et al. 2004) covering the 510 to 6500 cm^{-1} region at a resolution of around 0.06 cm^{-1} for temperatures of 5, 25, and 50°C. Generally speaking, sulphur chemistry is expected to play a key role in the formation of hazes and clouds in the atmospheres of exoplanets (Hobbs et al. 2021) with OCS an essential atmospheric molecule. It is often considered in the context of potential biosignature gases in the search for life elsewhere (Domagal-Goldman et al. 2011; Seager et al. 2012; Seager & Bains 2015), although it can be produced abiotically, for example, through atmospheric oxidation of CS_2.

In this work, a new OCS molecular line list suitable for high-temperature environments is presented. The line list, named OYT8, has been computed for the ExoMol database (Tennyson et al. 2020, 2016; Tennyson & Yurchenko 2012), which provides dedicated molecular spectroscopic data for modelling the atmospheres of exoplanets and other hot astronomical bodies. A line list of OCS is a valuable addition to ExoMol along with the other sulphur-bearing species it currently offers such as SO (Brady et al. 2024), SO_2 (Underwood et al. 2016a), SO_3 (Underwood et al. 2016b), H_2S (Azzam et al. 2016) and H_2CS (Mellor et al. 2022). There is increased interest in sulphur-bearing molecules on exoplanets after the recent discovery of SO_2 on Wasp-39b (Tsai et al. 2023; Powell et al. 2024), a molecule which can only be produced through photochemical processess. Photochemistry drives reactions in the atmosphere providing essential insights into the conditions on a planet. Future observations will target SO_2 so there is a high likelihood to observe OCS using the new ExoMol OYT8 line list.

The paper is structured as follows: In Sec. 2, we describe the theoretical molecular spectroscopic model and computational setup used to produce the new OCS line list. This entails details on the potential energy surface, dipole moment surface, variational calculations, temperature- and pressure-dependent molecular opacities, and "MARVELisation" of the line list to make it suitable for high-resolution applications. Sec. 3 presents results including details on the format of the line list, the temperature-dependent partition function of OCS, and simulated spectra compared against the current, best available OCS line list from the HITRAN database. Concluding remarks are given in Sec. 4.

2 METHODS

The ExoMol computational procedure for generating molecular line lists is well established (Tennyson 2016; Tennyson & Yurchenko 2017). For the rovibrational line list of OCS, calculations required an accurate molecular potential energy surface (PES), dipole moment surface (DMS), and variational nuclear motion program to solve the Schrödinger equation to obtain rovibrational energy levels and all possible transition probabilities between them.

2.1 Potential energy surface

A highly accurate PES of the electronic ground state of OCS has been utilised in the present work. Full details of its construction and validation have been reported elsewhere (Owens 2024), and only a summary is provided here. The PES was computed using state-of-the-art electronic structure calculations that treated a number of additional higher-level contributions to improve the *ab initio* accuracy. A sixth-order polynomial expansion was employed to represent the PES, and this analytic function was subsequently refined to a comprehensive list of empirically-derived rotation-vibration (rovibrational) energy levels up to $J = 10$, where J is the total angular momentum quantum number. This list had been established from an exhaustive analysis of the literature on high-resolution spectra of OCS (Xu & Tennyson 2023), discussed further in Sec. 2.4. The PES reproduced 434 energies below $hc \cdot 5000$ cm^{-1} (h is the Planck constant and c is the speed of light) with a root-mean-square (rms) error of 0.016 cm^{-1}, and 884 energy levels below 14 000 cm^{-1} with an rms error of 0.060 cm^{-1}, demonstrating unprecedented accuracy. The OCS PES is provided as supplementary material to this work.

2.2 Dipole moment surface

A newly computed *ab initio* DMS has been produced for this work. Calculations were performed with the quantum chemistry program MOLPRO2015 (Werner et al. 2012, 2020) using the coupled cluster method CCSD(T) in conjunction with the correlation consistent basis set aug-cc-pV5Z(+d for S) (Kendall et al. 1992; Dunning Jr. et al. 2001) in the frozen core approximation. The two dipole moment surfaces were constructed on a grid of 6037 nuclear geometries in terms of three internal coordinates: the O–C bond length $0.95 \leqslant r_{OC} \leqslant 1.58$ Å the C–S bond length $1.27 \leqslant r_{CS} \leqslant 2.46$ Å and the interbond angle $107.5 \leqslant \alpha \leqslant 180.0°$. This covered energies up to $hc \cdot 30\,000$ cm^{-1}. The C atom was fixed at the origin of the Cartesian xyz axis system with the O atom lying in the $+z$ direction and the S atom in the $-z$ direction at linear geometries. At each nuclear geometry, an external electric field with components ±0.005 a.u. was applied along the x (perpendicular) and z (parallel) axes and the respective dipole moment components determined via central finite differences.

The *ab initio* DMS of OCS was represented analytically using the point-charge molecular bond form (Huang et al. 2014)

ORIGINAL UNEDITED MANUSCRIPT

Downloaded from https://academic.oup.com/mnras/advance-article/doi/10.1093/mnras/stae1110/7657811 by guest on 28 April 2024

given by projections on the molecular bond vectors $\vec{r}_1$ (CO) and $\vec{r}_2$ (CS):

$$\vec{\mu} = \mu_x \vec{i} + \mu_z \vec{k} = \mu_{\rm O} \vec{r}_1 + \mu_{\rm S} \vec{r}_2$$

where μ_x and μ_z are the *ab initio* DMSs representing the projection of the dipole moment vector on the xyz frame used in MOLPRO calculations (the μ_y component is always zero). The two point-charge dipole moment components $\mu_{\rm O}$ and $\mu_{\rm S}$ were represented in terms of the vibrational coordinates,

$$\zeta_1 = r_1 - r_1^{\rm ref}, \quad (1)$$

$$\zeta_2 = r_2 - r_2^{\rm ref}, \quad (2)$$

$$\zeta_3 = \cos\alpha - 1, \quad (3)$$

where the stretching coordinates $r_1 = r_{\rm OC}$, $r_2 = r_{\rm CS}$, the interbond angle $\alpha = \angle({\rm OCS})$, and the reference parameters $r_1^{\rm req}$ and $r_2^{\rm req}$ were chosen to be similar to the equilibrium values of the PES of OCS around the linear configuration of the molecule (i.e. $\alpha_{\rm ref} = \pi$). The following analytic Taylor-type expansions were employed, (see e.g. Huang et al. (2014)):

$$\mu_{\rm O} = \sum_{ijk} F_{ijk}^{\rm (O)} \zeta_1^i \zeta_2^j \zeta_3^k, \quad (4)$$

and

$$\mu_{\rm S} = \sum_{ijk} F_{ijk}^{\rm (S)} \zeta_1^j \zeta_2^i \zeta_3^k, \quad (5)$$

with maximum expansion order $i+j+k = 6$. The expansion parameters $F_{ijk}^{\rm (O/S)}$ were established in a least-squares fitting to the *ab initio* data, which was weighted to favour geometries with energies below 16 000 cm^{-1} by using the Partridge and Schwenke weighting function (Partridge & Schwenke 1997) and Watson's robust fitting scheme (Watson 2003). The $\mu_{\rm O}$ component was fitted using 75 parameters (including the three equilibrium parameters) and reproduced the *ab initio* data with a weighted rms error of 9.0×10^{-6} Debye. The $\mu_{\rm S}$ component required 80 parameters (including the equilibrium parameters) and achieved a weighted rms error of 5.7×10^{-3} Debye. The expansion parameters of the OCS DMSs are given as supplementary material along with a Fortran routine to construct the analytic representations.

2.3 Variational calculations

Variational rovibrational calculations of OCS were performed using the computer program TROVE (Yurchenko et al. 2007), which is used extensively by the ExoMol database (Tennyson & Yurchenko 2012; Tennyson et al. 2016, 2020) for generating polyatomic molecular line lists. The general methodology of TROVE is well documented (Yurchenko et al. 2007, 2009; Yachmenev & Yurchenko 2015; Tennyson & Yurchenko 2017; Yurchenko et al. 2017; Yurchenko & Mellor 2020; Mellor et al. 2021) and details of the approach for treating linear and quasi-linear molecules can be found in Yurchenko & Mellor (2020). The spectra of several triatomic molecules have been computed with TROVE including CO_2 (Yurchenko et al. 2020), SiO_2 (Owens et al. 2020), CaOH (Owens et al. 2021a), KOH and NaOH (Owens et al. 2021b) (amongst numerous other larger polyatomics). The main steps of the line list calculations for OCS were as follows.

The rovibrational Schrödinger equation in the ground electronic state was solved with the exact kinetic energy operator for triatomic molecules (Yurchenko & Mellor 2020) based on the bisector embedding (Carter et al. 1983; Sutcliffe & Tennyson 1991), with the potential energy operator represented by a sixth-order power-series expansion. The vibrational basis set was built using a multi-step contraction scheme (Yurchenko et al. 2017) based on products of one-dimensional basis functions ϕ_{n_1}, ϕ_{n_2} and $\phi_{n_3}^L$ associated with the three vibrational modes of OCS. In TROVE, the two stretching and one bending vibrational mode have the respective quantum numbers n_1, n_2 and n_3, with L being the vibrational angular momentum quantum number associated with the bending mode. The primitive one-dimensional functions were determined numerically through solution of one-dimensional Schrödinger equations for each mode (stretch or bend) with all other modes set to their equilibrium values. The Numerov-Cooley method (Noumerov 1924; Cooley 1961) was utilised for the stretches on grids of 1000 points each, while the bending mode used associated Laguerre polynomials as a basis and a grid of 8000 points. The total size of the vibrational basis set was restricted by the polyad number condition $2(n_1 + n_2) + n_3 \leqslant 58$.

The final rovibrational basis set was established from symmetrized products of the symmetry-adapted vibrational $J = 0$ basis functions and symmetry-adapted rigid rotor functions $|J, k, m\rangle$, classified according to the irreducible representations of the $\boldsymbol{C}_{\rm s}$(M) molecular group symmetry (Bunker & Jensen 1998). Here, J is the total angular momentum quantum number, k and m are the rotational quantum numbers associated with the projection of the rotational angular momentum onto the molecular z and laboratory Z axes (in units of $\hbar$), respectively. An energy cut-off of $E = 40\,000$ cm^{-1} was used to contract the $J = 0$ eigenfunctions for states up to $K = |k| \leqslant 20$. Calculations employed atomic mass values of 15.99491463 Da (oxygen), 12.0 Da (carbon), and 31.9720707 Da (sulphur).

All energies and eigenfunctions up to $J = 223$ with energy below $hc \cdot 20\,000$ cm^{-1} (above the zero-point energy, computed to be 2014.537 cm^{-1} for OCS) were stored and used in intensity calculations. Transitions were considered in the 0 – 10 000 cm^{-1}

ORIGINAL UNEDITED MANUSCRIPT

Downloaded from https://academic.oup.com/mnras/advance-article/doi/10.1093/mnras/stae1110/7657811 by guest on 28 April 2024

range (wavelengths $\lambda > 1$ μm) for a lower state energy threshold of $hc \cdot 10\,000$ cm^{-1}. The final OCS OYT8 line list contains 2 482 380 391 transitions between 2 399 110 rovibrational states.

2.4 MARVELisation of the line list

Recently, an exhaustive review of published, high-resolution laboratory spectroscopic data of OCS was undertaken (Xu & Tennyson 2023), resulting in 14 071 independently measured and assigned rovibrational transitions being extracted and analysed using the MARVEL (Measured Active Rotational-Vibrational Energy Levels) procedure (Furtenbacher et al. 2007; Császár et al. 2007; Furtenbacher & Császár 2012; Tennyson et al. 2024). MARVEL takes a user-constructed dataset of assigned spectroscopic transitions with measurement uncertainties and inverts them to yield a consistent set of empirically-derived energy levels with quantum number labelling and uncertainties. For OCS, 13 056 of the extracted transitions were validated to produce a list of 5791 rovibrational energy levels up to $J = 96$ with energies below 14 551 cm^{-1}.

As mentioned earlier, the OCS MARVEL dataset was used to empirically refine the PES used in this study (Owens 2024), vastly improving the accuracy of the theoretical spectroscopic model, notably the computed rovibrational energy levels and hence transition wavenumbers. Further improvements in the accuracy of the OYT8 line list have been obtained through a procedure known as "MARVELisation", where the computed energy levels of the line list are replaced by the empirically-derived MARVEL values where available. For the OYT8 line list, 5655 energy levels were successfully matched and replaced up to $J = 96$ with energies below 14 551 cm^{-1}. This resulted in 354 830 transitions of the OYT8 line list being of experimental quality, i.e. highly accurate, with 105 922 of these having an intensity stronger than 10^{-28} cm/molecule at room temperature. The final OYT8 line list is therefore suitable for studying exoplanet atmospheres at high spectral resolution (Snellen 2014; Birkby 2018) in certain spectral windows. The adaptation of molecular line lists in the ExoMol database for high-resolution spectroscopy has become an integral part of ExoMol line list production, for example, see Bowesman et al. (2021).

2.5 ExoMolOP OCS opacities

To facilitate user adoption in the exoplanet community, temperature- and pressure-dependent molecular opacities of OCS based on the OYT8 line list have been generated using the ExoMolOP procedure (Chubb et al. 2021) for four exoplanet atmospheric retrieval codes: ARCiS (Min et al. 2020), TauREx (Al-Refaie et al. 2021), NEMESIS (Irwin et al. 2008) and petitRADTRANS (Mollière et al. 2019). ExoMolOP opacity calculations employed a temperature grid of 27 values [100, 200, 300, 400, 500, 600, 700, 800, 900, 1000, 1100, 1200, 1300, 1400, 1500, 1600, 1700, 1800, 1900, 2000, 2200, 2400, 2600, 2800, 3000, 3200, 3400] K, and a pressure grid of $[1 \times 10^{-5}, 2.15443469 \times 10^{-5}, 4.64158883 \times 10^{-5}, 1 \times 10^{-4}, 2.15443469 \times 10^{-4}, 4.64158883 \times 10^{-4}, 1 \times 10^{-3}, 2.15443469 \times 10^{-3}, 4.64158883 \times 10^{-3}, 1 \times 10^{-2}, 2.15443469 \times 10^{-2}, 4.64158883 \times 10^{-2}, 1 \times 10^{-1}, \times 10^{-1}, 4.64158883 \times 10^{-1}, 1, 2.15443469, 4.64158883, 10, 21.5443469, 46.4158883, 100]$ bar. For the line broadening, we assumed an 86% H_2 and 14% He atmosphere and Voigt line profile utilising the H_2 and He broadening parameters generated for the ExoMol database (Barton et al. 2017) based on Wilzewski et al. (2016).

3 RESULTS

3.1 Line list format

The OYT8 line list is provided in the ExoMol data format (Tennyson et al. 2020) by two file types. The `.states` file contains all of the computed rovibrational energy levels (in cm^{-1}), each possessing an uncertainty (in cm^{-1}), unique identifying quantum numbers, and a label in the final column indicating whether the energy level is calculated (`Ca`) or from the MARVEL empirically-derived dataset (`Ma`). An example of the `.states` file for OCS is given in Table 1 along with a description of each column.

Vibrational states have been labelled using the standard spectroscopic normal mode quantum numbers $v_1, v_2^{L_2}$ and v_3 for linear triatomic molecules. In OCS, the fundamentals are the C–S stretch ν_1 at ≈ 859 cm^{-1}, the bending mode ν_2 at ≈ 520 cm^{-1}, and the C–O stretch ν_3 at ≈ 2062 cm^{-1}. The additional vibrational angular momentum quantum number L_2 is needed to describe excitation of the ν_2 bending mode since motion can occur in two orthogonal planes with different phases. Also listed are the TROVE vibrational quantum numbers n_1, n_2, n_3 and L from the variational calculations, which were assigned by analysing the largest contribution from the underlying basis functions used to determine the energy level. These were correlated to the normal mode quantum numbers via the following rules: $v_1 = n_2$, $v_2^{L_2} = 2n_3 + L$, $v_3 = n_1$ and $L_2 = L$.

For energy levels replaced by a MARVEL value, the uncertainty was taken directly from the original MARVEL OCS dataset (Xu & Tennyson 2023). These states are highly accurate and transitions between them can be readily utilised in high-resolution studies. For all other energies, the uncertainties have been conservatively estimated using the expression,

$$\text{unc} = a(v_1 + v_2 + v_3) + bJ(J+1). \quad (6)$$

ORIGINAL UNEDITED MANUSCRIPT

Downloaded from https://academic.oup.com/mnras/advance-article/doi/10.1093/mnras/stae1110/7657811 by guest on 28 April 2024

Table 1. Extract from the `.states` file of the OCS OYT8 line list.

i	$\tilde{E}$	g_i	J	unc	$\Gamma_{\rm tot}$	v_1	v_2	L_2	v_3	e/f	$\Gamma_{\rm vib}$	$\Gamma_{\rm rot}$	C_i	n_1	n_2	n_3	Calc	Label
1	0.000000	1	0	0.000001	A′	0	0	0	0	e	A′	A′	1.00	0	0	0	0.000000	Ma
2	858.966914	1	0	0.000043	A′	1	0	0	0	e	A′	A′	1.00	0	1	0	858.960983	Ma
3	1047.042051	1	0	0.000001	A′	0	2	0	0	e	A′	A′	1.00	0	0	1	1047.038356	Ma
4	1710.976307	1	0	0.000127	A′	2	0	0	0	e	A′	A′	1.00	0	2	0	1710.978795	Ma
5	1892.228782	1	0	0.003530	A′	1	2	0	0	e	A′	A′	1.00	0	1	1	1892.240902	Ma
6	2062.201208	1	0	0.005020	A′	0	0	0	1	e	A′	A′	1.00	1	0	0	2062.199616	Ma
7	2104.827662	1	0	0.000100	A′	0	4	0	0	e	A′	A′	1.00	0	0	2	2104.845150	Ma
8	2555.990547	1	0	0.005657	A′	3	0	0	0	e	A′	A′	1.00	0	3	0	2556.003622	Ma
9	2731.402878	1	0	2.000000	A′	2	2	0	0	e	A′	A′	1.00	0	2	1	2731.402878	Ca
10	2918.105133	1	0	0.005657	A′	1	0	0	1	e	A′	A′	1.00	1	1	0	2918.124813	Ma

i:	State counting number.
$\tilde{E}$:	State energy (in cm^{-1}).
g_i:	Total statistical weight, equal to $g_{\rm ns}(2J+1)$.
J:	Total angular momentumn quantum number.
unc:	Uncertainty (in cm^{-1}).
$\Gamma_{\rm tot}$:	Overall symmetry in $\boldsymbol{C}_{\rm s}$(M) (A' or A'');
v_1:	Symmetric stretching ν_1 mode vibrational quantum number.
v_2:	Bending ν_2 mode vibrational quantum number.
L_2:	Vibrational angular momentum quantum number $L_2 = \|l_2\|$ associated with ν_2 mode.
v_3:	Antisymmetric stretching ν_3 mode vibrational quantum number.
e/f:	Rotationless parity.
$\Gamma_{\rm vib}$:	Symmetry of vibrational contribution in $\boldsymbol{C}_{\rm s}$(M) (A' or A'');
$\Gamma_{\rm rot}$:	Symmetry of rotational contribution in $\boldsymbol{C}_{\rm s}$(M) (A' or A'');
C_i:	Largest coefficient used in the TROVE vibrational assignment.
n_1, n_2, n_3:	TROVE vibrational quantum numbers.
Calc:	Original TROVE calculated state energy (in cm^{-1}).
Label:	"Ma" for MARVEL, "Ca" for calculated.

Table 2. Extract from the `.trans` file of the OCS OYT8 line list.

f	i	A_{fi}
1574778	1567709	2.16280036E-08
1271796	1263693	3.45517658E-12
725535	752181	3.31547603E-02
1643353	1625020	2.17082814E-05
529046	500544	1.77937507E-12

f: Upper state counting number;
i: Lower state counting number;
A_{fi}: Einstein-A coefficient (in s^{-1}).

Here, v_1, v_2 and v_3 correspond to the normal mode vibrational quantum numbers, J is the total angular momentum quantum number of the state, and the constants $a = 0.5$ and $b = 0.01$ cm^{-1}. The uncertainty increases for increasing levels of vibrational and rotational excitation, so higher energy states are presumed less accurate. However, in many instances the energy levels will be more accurate than the uncertainty suggests but we want to ensure users can easily differentiate between the high-resolution levels and those not adapted.

In Table 2, an extract from one of the `.trans` files is shown, which lists computed transitions via upper and lower state ID running numbers, and Einstein A coefficients (in s^{-1}). For ease of use the OYT8 line list has been split into 10 transition files covering the 0 – 10 000 cm^{-1} range.

3.2 Temperature-dependent partition function

Knowledge of the temperature-dependent partition function $Q(T)$ is needed for simulations of rovibrational line intensities. For OCS, $Q(T)$ was calculated on a 1 K grid in the 1 – 5000 K range (available with the line list from the ExoMol website) using the expression,

$$Q(T) = \sum_i g_i \exp\left(-\frac{hc \cdot E_i}{kT}\right). \quad (7)$$

ORIGINAL UNEDITED MANUSCRIPT

Downloaded from https://academic.oup.com/mnras/advance-article/doi/10.1093/mnras/stae1110/7657811 by guest on 28 April 2024

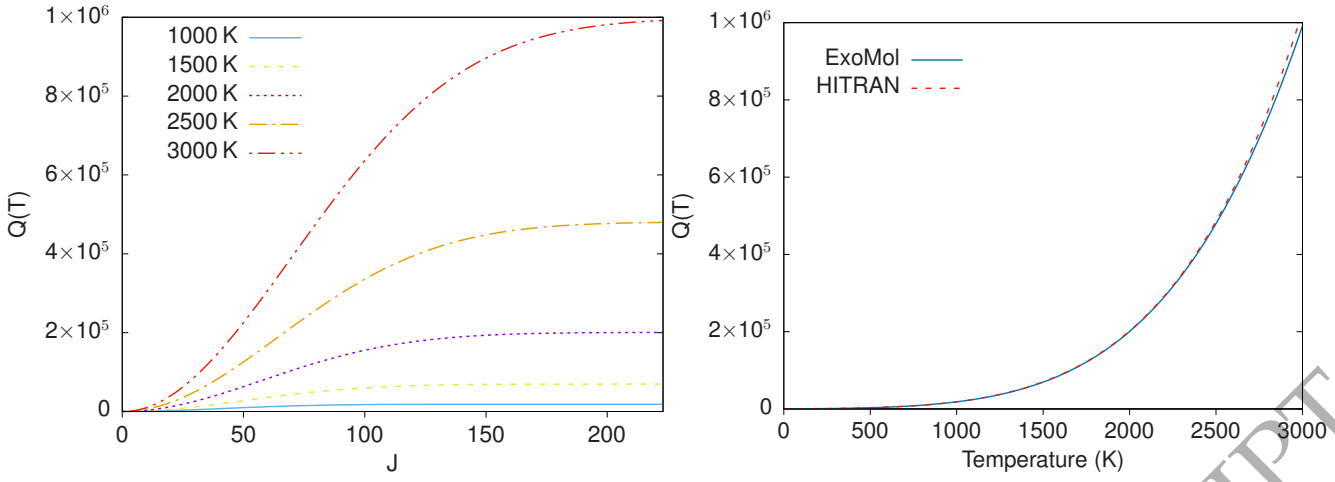

Figure 1. The left panel shows the convergence of the temperature-dependent partition function $Q(T)$ of OCS with respect to the total angular momentum quantum number J at various temperatures (in Kelvin). The right panel is a comparison of $Q(T)$ against partition function values from the HITRAN database (Gordon et al. 2022), determined using the Total Internal Partition Sums (TIPS) method (Gamache et al. 2021).

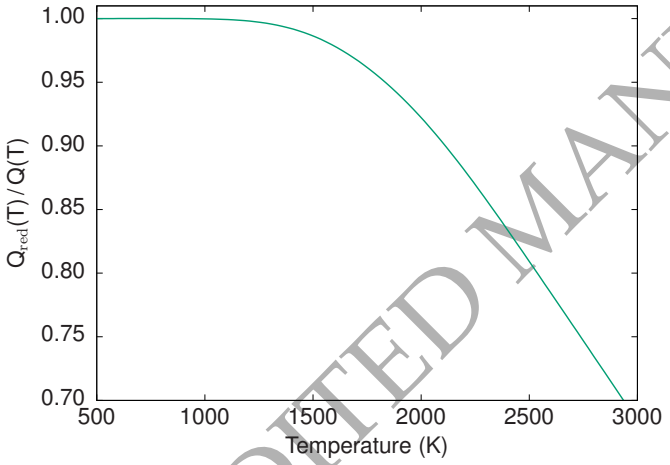

Figure 2. Illustration of the ratio $Q_{\rm red}(T)/Q(T)$ with respect to temperature T; this measure gives insight into the completeness of the OCS line list. A soft temperature limit of $T = 2000$ K is recommended for the line list without significant loss of opacity.

Here, $g_i = g_{\rm ns}(2J_i+1)$ is the degeneracy of a state i with energy E_i (in cm^{-1}) and total angular momentum quantum number J_i, with the nuclear spin statistical weight $g_{\rm ns} = 1$ for ^{16}O^{12}C^{32}S, h is the Planck constant, c is the speed of light, k is the Boltzmann constant and T is the temperature. Values were obtained by summing over all of the computed rovibrational energy levels of the OYT8 line list.

In Fig. 1, the convergence of $Q(T)$ as a function of J at different temperatures is shown (left panel) along with a comparison of $Q(T)$ against values from the HITRAN molecular spectroscopic database (Gamache et al. 2017) up to 3000 K (right panel). The partition function converges quickly up to 2000 K, but above this convergence slows and by 3000 K is not fully converged, indicating that higher J states above $J > 223$ are needed for the line list to be complete at this temperature. When compared against values from HITRAN determined using the Total Internal Partition Sums (TIPS) approach (Gamache et al. 2017), our $Q(T)$ values are in excellent agreement and only show slight deviations approaching 3000 K, which is beyond the recommended temperature limit of the OYT8 line list.

The OYT8 line list was computed with a lower state energy threshold of $hc \cdot 10\,000$ cm^{-1}. Further insight into its completeness is possible through calculation of the reduced partition function $Q_{\rm red}(T)$, which only considers energy levels up to $hc \cdot 10\,000$ cm^{-1} in the summation of Eq. (7). The ratio $Q_{\rm red}(T)/Q(T)$ is plotted with respect to temperature in Fig. 2. At lower temperatures this measure equals unity and demonstrates completeness of the line list as the partition function does not change because of the lower state energy threshold. However, as the temperature increases this ratio starts to decrease and $Q_{\rm red}/Q \approx 0.92$ at 2000 K, dropping considerably to 0.68 at 3000 K. We therefore recommend $T = 2000$ K as a soft temperature limit for the OYT8 line list and expect that use above this temperature will result in a progressive loss of opacity.

ORIGINAL UNEDITED MANUSCRIPT

Downloaded from https://academic.oup.com/mnras/advance-article/doi/10.1093/mnras/stae1110/7657811 by guest on 28 April 2024

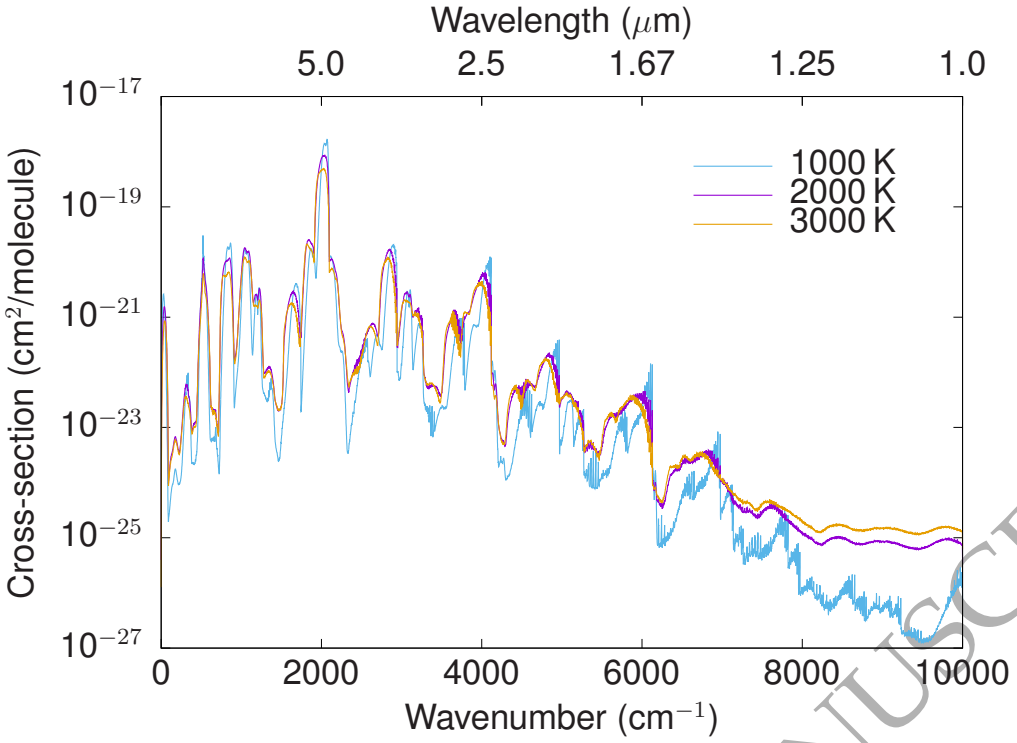

Figure 3. Simulated temperature-dependent OCS spectra using the OYT8 line list. Absorption cross-sections were computed at a resolution of 1 cm^{-1} and modelled with a Gaussian line profile with a half width at half maximum (HWHM) of 1 cm^{-1} at high temperatures (in Kelvin). Intensities have not been scaled to natural abundance.

3.3 Simulated spectra

All spectral simulations were performed using the ExoCross computer program (Yurchenko et al. 2018b), which is based on the methodology of Hill et al. (2013). ExoCross is a highly efficient code capable of generating spectra with a variety of line shapes and conditions at arbitrary temperatures. We mention that zero-pressure cross-sections of OCS can be readily produced using the ExoMol cross-sections app at `www.exomol.com` for any temperature between 100 K and 5000 K, see Hill et al. (2013).

In Fig. 3, the temperature dependence of the OCS spectrum is shown, where we have simulated absorption cross-sections at three temperature ($T = 1000, 2000, 3000$ K) at a resolution of 1 cm^{-1} and modelled with a Gaussian line profile with a half width at half maximum (HWHM) of 1 cm^{-1}. The strongest band of OCS is the ν_3 C–O stretching mode at approximately 2062 cm^{-1} (wavelengths $\lambda \approx 4.85$ μm), which remains the most intense feature at all temperatures. As expected, the rotational bands broaden with increasing temperature caused by the increased population in the vibrationally excited states, resulting in a flatter and smoother spectrum.

Exoplanetary studies searching for OCS (Tsai et al. 2023; Alderson et al. 2023) are currently using the line list from the HITRAN database (Gordon et al. 2022), which contains 21 776 transitions for the main isotopologue ^{16}O^{12}C^{32}S in the 0 – 8000 cm^{-1} region (wavelengths $\lambda > 1.25$ μm). In Fig. 4, we have plotted all of the HITRAN ^{16}O^{12}C^{32}S data against the OYT8 line list at a temperature of $T = 296$ K, employing an intensity threshold of 10^{-28} cm/molecule for this comparison. In the Solar System, the main isotopologue ^{16}O^{12}C^{32}S is approximately 93.74% abundant (with ^{16}O^{12}C^{34}S the second most abundant at 4.16%) so we have scaled the OYT8 line intensities by 0.9374 to compare with HITRAN. Overall, the OYT8 line list possesses far superior coverage, showing good agreement with HITRAN but with slight discrepancies in the strength of the intensities for a small number of bands. The line list of OCS in the HITRAN database has a somewhat convoluted history, see the OCS section in the HITRAN database papers from the year 2000 onwards (Rothman et al. 2003, 2005, 2009, 2013; Gordon et al. 2017, 2022), with some of the data taken from private communications and the intensities of certain bands being scaled based on measurements of other bands.

In Figs. 5 and 6, we focus on many of the OCS spectroscopic bands in the HITRAN database. The pure rotational and fundamental bands are shown in Fig. 5. There is excellent agreement for the stretching modes, especially for the strongest ν_3 C–O stretching mode at approximately 2062 cm^{-1} (wavelengths $\lambda \approx 4.85$ μm). However, the intensity of the bending ν_2 mode at ≈ 520 cm^{-1} ($\lambda \approx 19.23$ μm) in the OYT8 line list is around a factor of 1.5 stronger than the HITRAN database and may indicate a potential issue. The HITRAN intensities of the ν_2 mode are based on older intensity measurements of

ORIGINAL UNEDITED MANUSCRIPT

Downloaded from https://academic.oup.com/mnras/advance-article/doi/10.1093/mnras/stae1110/7657811 by guest on 28 April 2024

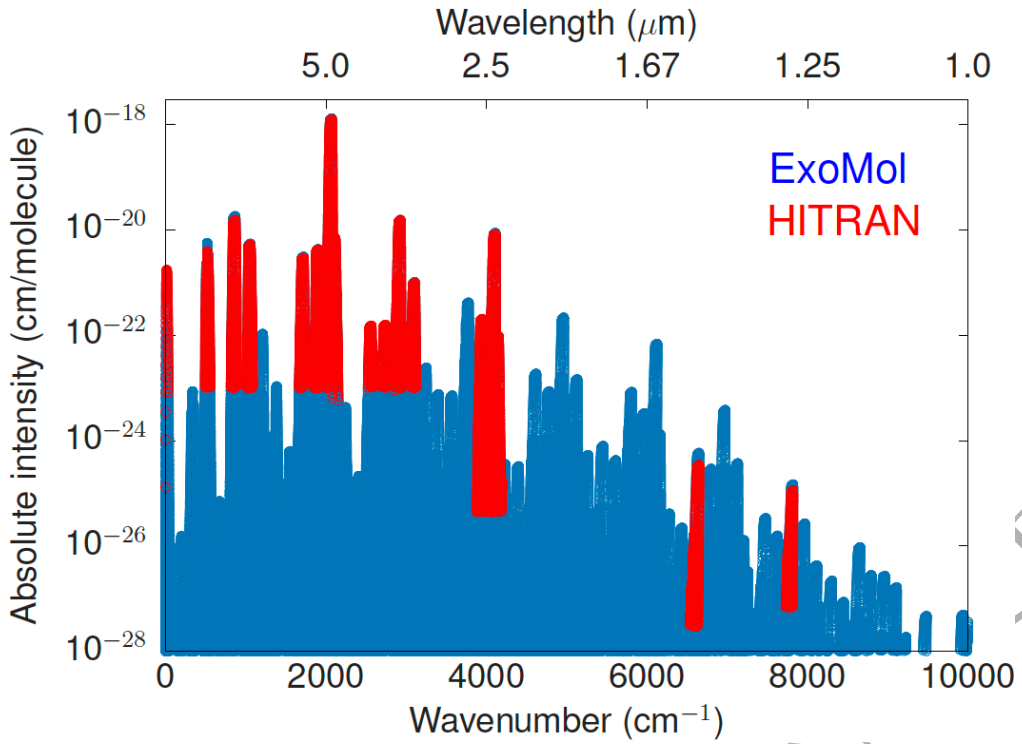

Figure 4. Overview of the coverage of the ExoMol OYT8 line list compared against all transitions of $^{16}O^{12}C^{32}S$ from the HITRAN database (Gordon et al. 2022). The ExoMol OYT8 line intensities have been computed at $T = 296$ K and scaled by 0.9374 (natural abundance). An intensity threshold of 10^{-28} cm/molecule was applied for this figure.

Kagann (1982) that have since been replaced for the other fundamental bands with more accurate values, but not for the ν_2 region. Given the agreement of the OYT8 line list intensities with the other fundamentals, and with the excited $2\nu_2$ mode at ≈ 1047 cm^{-1} ($\lambda \approx 9.55$ μm) shown in Fig. 6, we are confident in the accuracy of the OYT8 line list and the underlying *ab initio* DMSs utilised in this work. It is widely accepted that transition intensities computed using *ab initio* DMSs are comparable to, if not occasionally more reliable, than experiment (Yurchenko 2014; Tennyson 2014) (well within 5–10% of experimentally determined values). Weaker combination and overtone bands are compared in Fig. 6, and again, the agreement is excellent. Most impressive are the bands in the regions around ≈ 6630 cm^{-1} ($\lambda \approx 1.51$ μm) and ≈ 7800 cm^{-1} ($\lambda \approx 1.28$ μm), which have very weak intensities of the order 10^{-25} cm/molecule and below.

In Fig. 7, we have simulated absorption cross-sections at $T = 296$ K (scaled to natural abundance) modelled with a Gaussian line profile with a HWHM of 0.135 cm^{-1} at a resolution of 0.06 cm^{-1}. This line shape is a reasonable estimate for comparisons against the PNNL spectral library (Sharpe et al. 2004). The PNNL OCS spectrum was measured in the laboratory at a temperature of 25°C with the dataset subsequently re-normalized to room temperature (296 K). The stated purity of the measured OCS gas is 97.5% but it is flagged as doubtful since $\approx 25\%$ CO_2 and 5% CO were present in the sample. The effect of these impurities is confirmed in the bottom right panel of Fig. 7, where a large spectroscopic feature in the PNNL OCS spectrum is detected that is not present in the OYT8 line list. Carbon disulphide (CS_2) possesses an antisymmetric stretching fundamental mode at ≈ 1535 cm^{-1} (Davies & Orville-Thomas 1969), which we believe is the cause of this feature. The ν_2 bending fundamental band of OCS at ≈ 520 cm^{-1} is also not properly captured by PNNL as their experiment only measured transitions above 510 cm^{-1}, hence missing vital contributions to this band. Otherwise, the OYT8 absorption cross-sections are in good agreement with the experimentally determined PNNL spectrum.

As a final comparison, in Fig. 8 absolute line intensities (above a threshold of 1×10^{-28} cm/molecule) at $T = 296$ K of the ExoMol OYT8 line list are shown alongside a computed NASA AMES OCS line list from the NASA AMES molecular spectroscopic database (retrieved from `https://huang.seti.org/OCS/ocs.html`; accessed March 2024). The NASA AMES OCS line list has not yet been formally published so we do not perform a detailed comparison. The AMES line list was computed using an empirically refined PES and high-level *ab initio* DMS, considering transitions in the 0 – 15 942 cm^{-1} range for rovibrational states up to $J = 150$ with a lower state energy threshold of 16 000 cm^{-1}. Overall, the structure of the two line lists is in good agreement and this comparison serves as further validation of our line list calculation procedure.

Finally, in Fig. 9 we have plotted the results of the MARVELisation procedure performed on the OYT8 line list. The replacement of 5655 computed energy levels with the corresponding MARVEL empirical-quality values resulted in 79 458 highly accurate transitions with an intensity stronger than 10^{-28} cm/molecule at room temperature. These transitions are suitable

ORIGINAL UNEDITED MANUSCRIPT

Downloaded from https://academic.oup.com/mnras/advance-article/doi/10.1093/mnras/stae1110/7657811 by guest on 28 April 2024

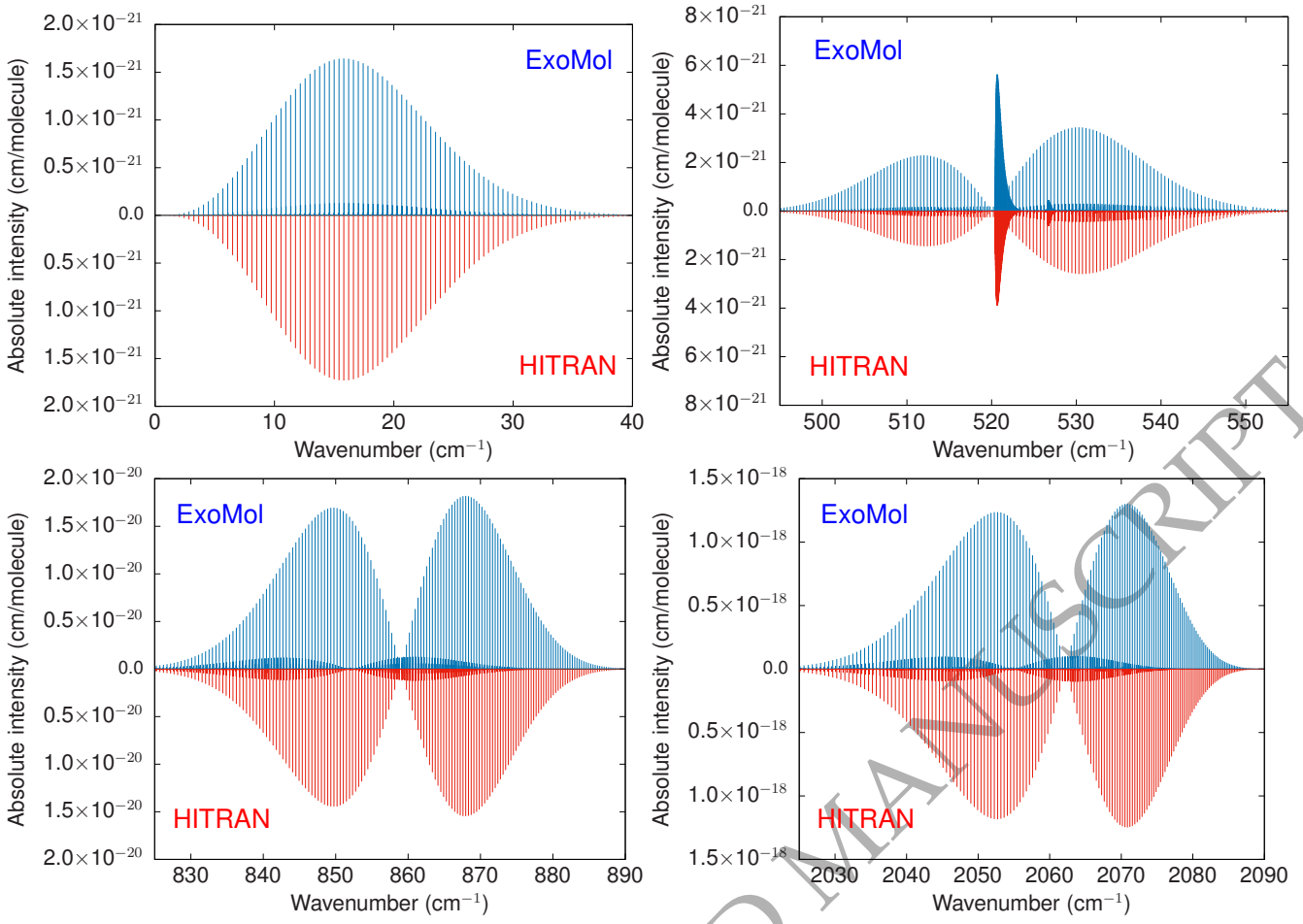

Figure 5. Absolute line intensities of the ExoMol OYT8 line list at $T = 296$ K compared against the HITRAN database (Gordon et al. 2022). The pure rotational band and three fundamental bands of OCS are shown, namely the C–S stretch ν_1 at ≈ 859 cm^{-1}, the bending mode ν_2 at ≈ 520 cm^{-1}, and the C–O stretch ν_3 at ≈ 2062 cm^{-1}. Note the ExoMol OYT8 intensities have been scaled by 0.9374 (natural abundance).

for high-resolution applications. Their coverage is shown in Fig. 9 and it is evident that the majority of strong spectroscopic features of OCS are covered by the MARVELisation procedure. The OCS OYT8 line list is extremely comprehensive, totalling just under 2.5 billion transitions between nearly 2.4 million states. We recommended its use in future exoplanetary studies.

4 CONCLUSIONS

A new molecular line list for the main isotopologue of carbonyl sulphide $^{16}O^{12}C^{32}S$ covering wavelengths $\lambda > 1$ μm (0–10 000 cm^{-1} range) has been presented. Containing almost 2.5 billion transitions between 2.4 million rovibrational states up to $J = 223$, the OYT8 line list is recommended for use with a 'soft' upper temperature limit of 2000 K. The line list was computed using the variational nuclear motion code TROVE utilising a highly accurate, empirically refined PES and newly computed *ab initio* DMS of OCS. Post-processing of the OYT8 line list was undertaken by replacing calculated energy levels with empirically-derived values where available, a process known as MARVELisation. A total of 79 458 lines of the OYT8 line list (with an intensity stronger than 10^{-28} cm/molecule at room temperature) are of experimental quality, covering the most important OCS spectroscopic features and making the OYT8 line list suitable for high-resolution applications. Overall, the OYT8 line list displayed excellent agreement with the OCS line list from the HITRAN database despite discrepancies in the ν_2 band line intensities, the PNNL spectral library, and the NASA AMES computed OCS line list.

The strongest infrared feature of OCS corresponds to the ν_3 C–O stretching fundamental band at around 2062 cm^{-1} (wavelengths $\lambda \approx 4.85$ μm), which was considered in the recent study of Wasp-39b (Alderson et al. 2023) but overlapping opacity with CO and H_2S in their model made it challenging to conclusively detect OCS. The increased coverage of the OYT8 line list and the many new spectroscopic features that are available will greatly facilitate the future observation of OCS on exoplanets. The OYT8 line list, along with the associated temperature- and pressure-dependent molecular opacities, can be

ORIGINAL UNEDITED MANUSCRIPT

Downloaded from https://academic.oup.com/mnras/advance-article/doi/10.1093/mnras/stae1110/7657811 by guest on 28 April 2024

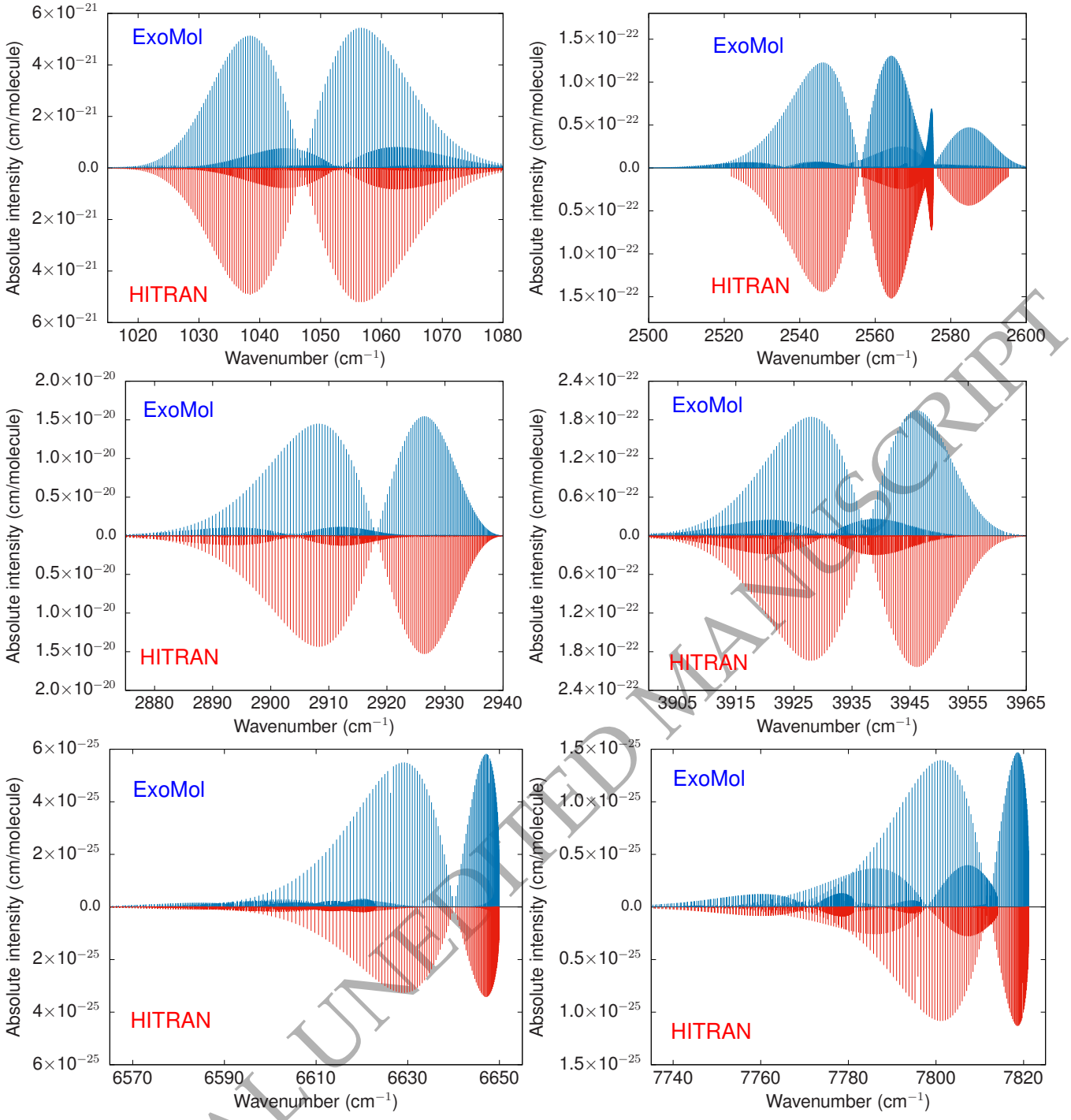

Figure 6. Absolute line intensities of the ExoMol OYT8 line list at $T = 296$ K compared against the HITRAN database (Gordon et al. 2022). Combination and overtone bands with weaker intensities are shown. Note the ExoMol OYT8 intensities have been scaled by 0.9374 (natural abundance).

freely downloaded from the ExoMol database at `www.exomol.com`. OCS joins a growing number of sulphur-bearing molecules available from ExoMol including SO (Brady et al. 2024), SO_2 (Underwood et al. 2016a), SO_3 (Underwood et al. 2016b), H_2S (Azzam et al. 2016), H_2CS (Mellor et al. 2022), CS (Paulose et al. 2015), PS (Prajapat et al. 2017), SiS (Upadhyay et al. 2018), SH (Gorman et al. 2019) and NS (Yurchenko et al. 2018a).

ORIGINAL UNEDITED MANUSCRIPT

Downloaded from https://academic.oup.com/mnras/advance-article/doi/10.1093/mnras/stae1110/7657811 by guest on 28 April 2024

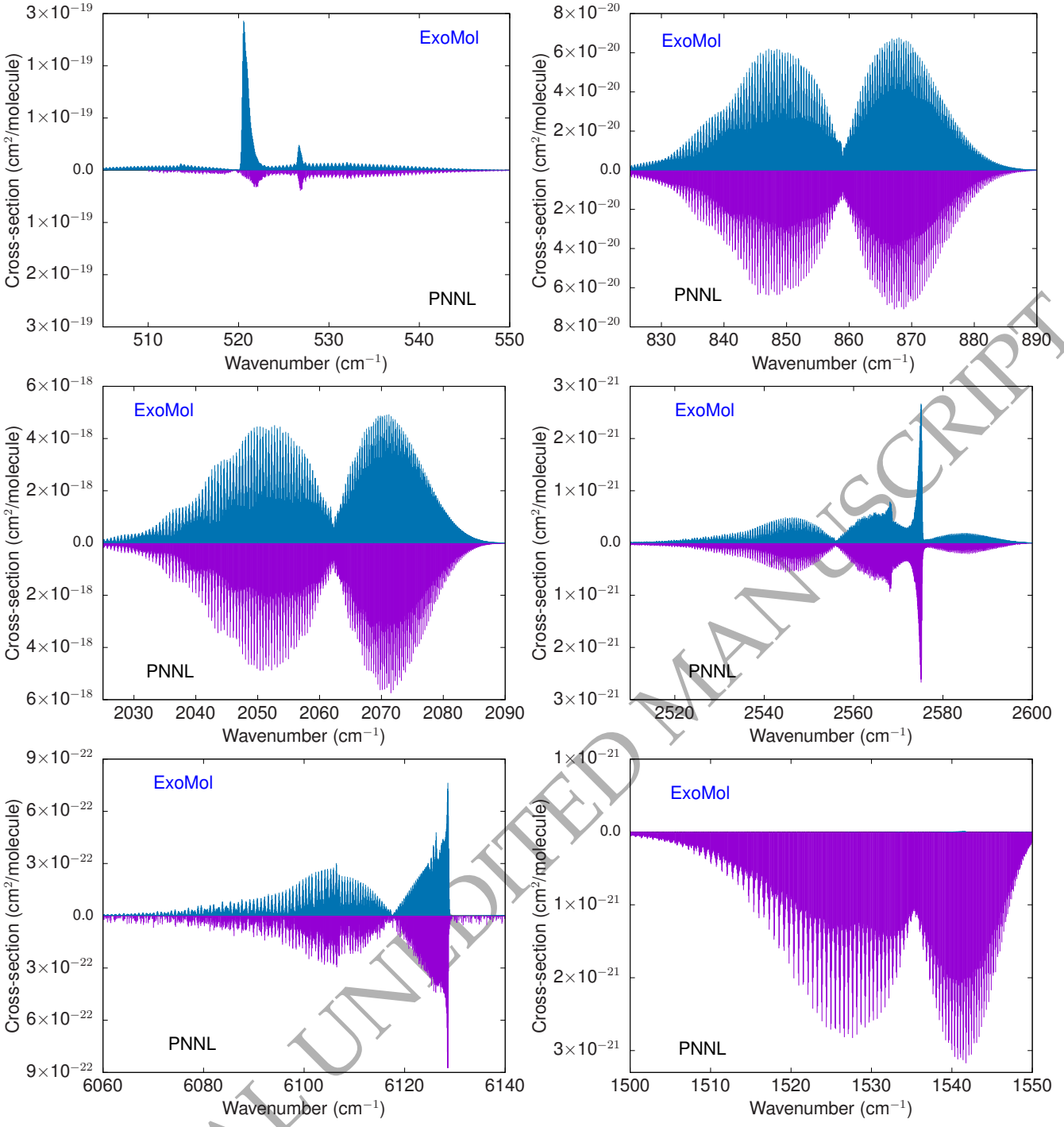

Figure 7. Absorption cross-sections of the ExoMol OYT8 line list at $T = 298$ K compared against the PNNL spectral library (Sharpe et al. 2004). The three fundamental bands of OCS are shown, namely the C–S stretch ν_1 at ≈ 859 cm^{-1}, the bending mode ν_2 at ≈ 520 cm^{-1}, and the C–O stretch ν_3 at ≈ 2062 cm^{-1}. In the bottom right panel, an impurity is seen in the experimental PNNL spectrum, which shows a strong spectroscopic feature attributed to the CS_2 molecule at ≈ 1535 cm^{-1}. Note the ExoMol OYT8 intensities have been scaled by 0.9374 (natural abundance).

ACKNOWLEDGMENTS

The authors are grateful to Iouli Gordon for valuable comments on our manuscript. This work was supported by the Science and Technology Facilities Council (STFC) Projects ST/W000504/1, and by the European Research Council (ERC) under the European Union's Horizon 2020 research and innovation programme through Advance Grant number 883830. AO acknowledges additional support from the Engineering and Physical Sciences Research Council [grant number EP/S021582/1]. The authors acknowledge the use of the UCL Myriad High Performance Computing Facility and associated support services in

ORIGINAL UNEDITED MANUSCRIPT

Downloaded from https://academic.oup.com/mnras/advance-article/doi/10.1093/mnras/stae1110/7657811 by guest on 28 April 2024

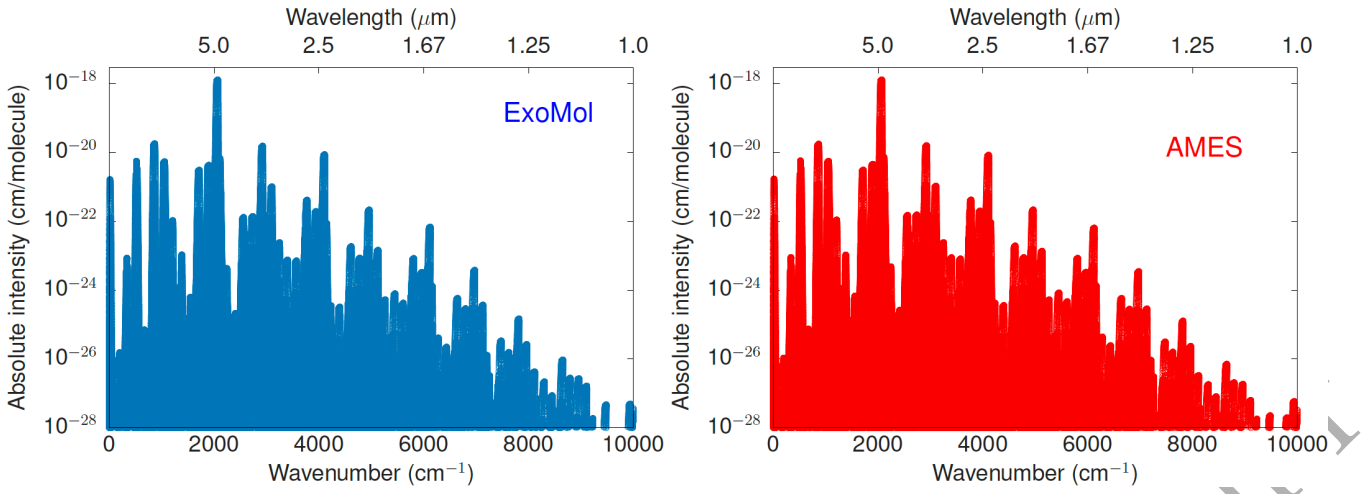

Figure 8. Overview of the coverage of the ExoMol OYT8 line list (left panel) and the NASA AMES $^{16}O^{12}C^{32}S$ line list (right panel). The NASA AMES line list was downloaded from https://huang.seti.org/OCS/ocs.html (accessed March 2024). Both the ExoMol OYT8 and AMES line intensities are at $T = 296$ K and scaled by 0.9374 (natural abundance). An intensity threshold of 10^{-28} cm/molecule was applied for this figure.

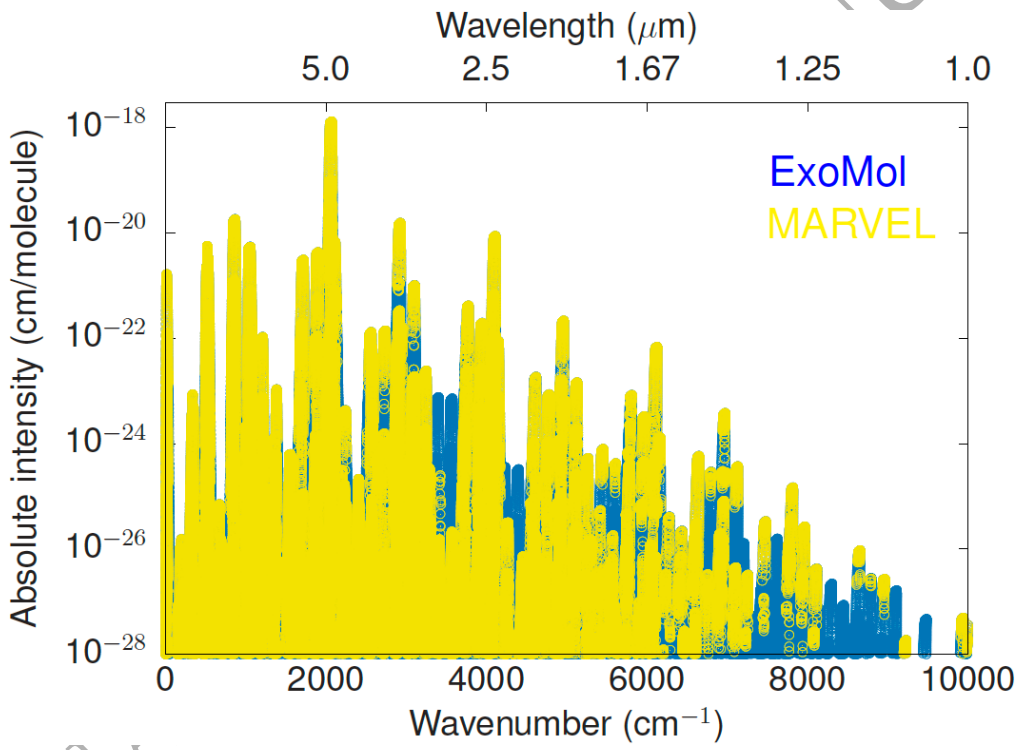

Figure 9. Overview of the coverage of the MARVEL empirical-quality lines compared to the ExoMol OYT8 line list. Both the MARVEL and ExoMol OYT8 line intensities have been computed at $T = 296$ K and scaled by 0.9374 (natural abundance). An intensity threshold of 10^{-28} cm/molecule was applied for this figure.

the completion of this work, along with the Cambridge Service for Data Driven Discovery (CSD3), part of which is operated by the University of Cambridge Research Computing on behalf of the STFC DiRAC HPC Facility (www.dirac.ac.uk). The DiRAC component of CSD3 was funded by BEIS capital funding via STFC capital grants ST/P002307/1 and ST/R002452/1 and STFC operations grant ST/R00689X/1. DiRAC is part of the National e-Infrastructure.

Downloaded from https://academic.oup.com/mnras/advance-article/doi/10.1093/mnras/stae1110/7657811 by guest on 28 April 2024

DATA AVAILABILITY

The states, transition, opacity and partition function files for the OCS line list can be downloaded from www.exomol.com and the CDS data centre cdsarc.u-strasbg.fr. The open access programs TROVE and ExoCross are available from github.com/exomol.

SUPPORTING INFORMATION

Supplementary data are available at MNRAS online. This includes the potential energy and dipole moment surfaces of OCS with programs to construct them.

REFERENCES

Al-Refaie A. F., Changeat Q., Waldmann I. P., Tinetti G., 2021, ApJ, 917, 37
Alderson L., et al., 2023, Nature, 614, 664
Azzam A. A. A., Yurchenko S. N., Tennyson J., Naumenko O. V., 2016, MNRAS, 460, 4063
Barton E. J., Hill C., Czurylo M., Li H.-Y., Hyslop A., Yurchenko S. N., Tennyson J., 2017, J. Quant. Spectrosc. Radiat. Transf., 203, 490
Birkby J. L., 2018, Handbook of Exoplanets, pp 1485–1508
Bowesman C. A., Shuai M., Yurchenko S. N., Tennyson J., 2021, MNRAS, 508, 3181
Brady R. P., Yurchenko S. N., Tennyson J., Kim G.-S., 2024, MNRAS, 527, 6675
Bunker P. R., Jensen P., 1998, Molecular Symmetry and Spectroscopy, 2 edn. NRC Research Press, Ottawa
Bézard B., de Bergh C., Crisp D., Maillard J.-P., 1990, Nature, 345, 508
Carter S., Handy N., Sutcliffe B., 1983, Mol. Phys., 49, 745
Chubb K. L., et al., 2021, A&A, 646, A21
Cooley J. W., 1961, Math. Comp., 15, 363
Császár A. G., Czakó G., Furtenbacher T., Mátyus E., 2007, Annu. Rep. Comput. Chem., 3, 155
Davies P., Orville-Thomas W., 1969, J. Mol. Struct., 4, 163
Domagal-Goldman S. D., Meadows V. S., Claire M. W., Kasting J. F., 2011, Astrobiology, 11, 419
Dunning Jr. T. H., Peterson K. A., Wilson A. K., 2001, J. Chem. Phys., 114, 9244
Furtenbacher T., Császár A. G., 2012, J. Mol. Struct., 1009, 123
Furtenbacher T., Császár A. G., Tennyson J., 2007, J. Mol. Spectrosc., 245, 115
Gamache R. R., et al., 2017, J. Quant. Spectrosc. Radiat. Transf., 203, 70
Gamache R. R., Vispoel B., Rey M., Nikitin A., Tyuterev V., Egorov O., Gordon I. E., Boudon V., 2021, J. Quant. Spectrosc. Radiat. Transf., 271, 107713
Gordon I. E., et al., 2017, J. Quant. Spectrosc. Radiat. Transf., 203, 3
Gordon I. E., et al., 2022, J. Quant. Spectrosc. Radiat. Transf., 277, 107949
Gorman M., Yurchenko S. N., Tennyson J., 2019, MNRAS, 490, 1652
Hill C., Yurchenko S. N., Tennyson J., 2013, Icarus, 226, 1673
Hobbs R., Rimmer P. B., Shorttle O., Madhusudhan N., 2021, MNRAS, 506, 3186
Huang X., Schwenke D. W., Lee T. J., 2014, J. Chem. Phys., 140, 114311
Irwin P. G. J., et al., 2008, J. Quant. Spectrosc. Radiat. Transf., 109, 1136
Jefferts K. B., Penzias A. A., Wilson R. W., Solomon P. M., 1971, ApJ, 168, L111
Kagann R. H., 1982, J. Mol. Spectrosc., 94, 192
Kendall R. A., Dunning T. H., Harrison R. J., 1992, J. Chem. Phys., 96, 6796
Khalil M. A. K., Rasmussen R. A., 1984, Atmos. Environ., 18, 1805
Lee C.-L., Brimblecombe P., 2016, Earth-Sci. Rev., 160, 1
Lellouch E., et al., 1995, Nature, 373, 592
Leman L., Orgel L., Ghadiri M. R., 2004, Science, 306, 283
Mauersberger R., Henkel C., Chin Y. N., 1995, A&A, 294, 23
McClure M. K., et al., 2023, Nat. Astron., 7, 431–443
Mellor T. M., Yurchenko S. N., Jensen P., 2021, Symmetry, 13, 548
Mellor T., Owens A., Yurchenko S. N., Tennyson J., 2022, MNRAS, 520, 1997
Min M., Ormel C. W., Chubb K., Helling C., Kawashima Y., 2020, A&A, 642, A28
Mollière P., Wardenier J. P., van Boekel R., Henning T., Molaverdikhani K., Snellen I. A. G., 2019, A&A, 627, A67
Noumerov B. V., 1924, MNRAS, 84, 592
Owens A., 2024, submitted
Owens A., Conway E. K., Tennyson J., Yurchenko S. N., 2020, MNRAS, 495, 1927
Owens A., Clark V. H. J., Mitrushchenkov A., Yurchenko S. N., Tennyson J., 2021a, J. Chem. Phys., 154, 234302
Owens A., Tennyson J., Yurchenko S. N., 2021b, MNRAS, 502, 1128
Partridge H., Schwenke D. W., 1997, J. Chem. Phys., 106, 4618
Paulose G., Barton E. J., Yurchenko S. N., Tennyson J., 2015, MNRAS, 454, 1931
Powell D., et al., 2024, Nature, 626, 979
Prajapat L., Jagoda P., Lodi L., Gorman M. N., Yurchenko S. N., Tennyson J., 2017, MNRAS, 472, 3648
Rothman L. S., et al., 2003, J. Quant. Spectrosc. Radiat. Transf., 82, 5
Rothman L. S., et al., 2005, J. Quant. Spectrosc. Radiat. Transf., 96, 139

ORIGINAL UNEDITED MANUSCRIPT

Downloaded from https://academic.oup.com/mnras/advance-article/doi/10.1093/mnras/stae1110/7657811 by guest on 28 April 2024

Rothman L. S., et al., 2009, J. Quant. Spectrosc. Radiat. Transf., 110, 533
Rothman L. S., et al., 2013, J. Quant. Spectrosc. Radiat. Transf., 130, 4
Seager S., Bains W., 2015, Sci. Adv., 1, e1500047
Seager S., Schrenk M., Bains W., 2012, Astrobiology, 12, 61
Sharpe S. W., Johnson T. J., Sams R. L., Chu P. M., Rhoderick G. C., Johnson P. A., 2004, Appl. Spectrosc., 58, 1452
Snellen I., 2014, Phil. Trans. Royal Soc. London A, 372, 20130075
Sutcliffe B. T., Tennyson J., 1991, Int. J. Quantum Chem., 39, 183
Tennyson J., 2014, J. Mol. Spectrosc., 298, 1
Tennyson J., 2016, J. Chem. Phys., 145, 120901
Tennyson J., Yurchenko S. N., 2012, MNRAS, 425, 21
Tennyson J., Yurchenko S. N., 2017, Int. J. Quantum Chem., 117, 92
Tennyson J., et al., 2016, J. Mol. Spectrosc., 327, 73
Tennyson J., et al., 2020, J. Quant. Spectrosc. Radiat. Transf., 255, 107228
Tennyson J., Furtenbacher T., Yurchenko S. N., Császár A. G., 2024, J. Quant. Spectrosc. Radiat. Transf., 316, 108902
Tsai S.-M., et al., 2023, Nature, 617, 483
Underwood D. S., Tennyson J., Yurchenko S. N., Huang X., Schwenke D. W., Lee T. J., Clausen S., Fateev A., 2016a, MNRAS, 459, 3890
Underwood D. S., Tennyson J., Yurchenko S. N., Clausen S., Fateev A., 2016b, MNRAS, 462, 4300
Upadhyay A., Conway E. K., Tennyson J., Yurchenko S. N., 2018, MNRAS, 477, 1520
Watson J. K. G., 2003, J. Mol. Spectrosc., 219, 326
Werner H.-J., Knowles P. J., Knizia G., Manby F. R., Schütz M., 2012, WIREs Comput. Mol. Sci., 2, 242
Werner H.-J., et al., 2020, J. Chem. Phys., 152, 144107
Wilzewski J. S., Gordon I. E., Kochanov R. V., Hill C., Rothman L. S., 2016, J. Quant. Spectrosc. Radiat. Transf., 168, 193
Woodney L., McMullin J., A'Hearn M., 1997, Planet. Space Sci., 45, 717
Xu E., Tennyson J., 2023, Mol. Phys., p. e2279694
Yachmenev A., Yurchenko S. N., 2015, J. Chem. Phys., 143, 014105
Yurchenko S. N., 2014, in , Vol. 10, Chemical Modelling: Volume 10. The Royal Society of Chemistry, pp 183–228, doi:10.1039/9781849737241-00183, http://dx.doi.org/10.1039/9781849737241-00183
Yurchenko S. N., Mellor T. M., 2020, J. Chem. Phys., 153, 154106
Yurchenko S. N., Thiel W., Jensen P., 2007, J. Mol. Spectrosc., 245, 126
Yurchenko S. N., Barber R. J., Yachmenev A., Thiel W., Jensen P., Tennyson J., 2009, J. Phys. Chem. A, 113, 11845
Yurchenko S. N., Yachmenev A., Ovsyannikov R. I., 2017, J. Chem. Theory Comput., 13, 4368
Yurchenko S. N., Bond W., Gorman M. N., Lodi L., McKemmish L. K., Nunn W., Shah R., Tennyson J., 2018a, MNRAS, 478, 270
Yurchenko S. N., Al-Refaie A. F., Tennyson J., 2018b, A&A, 614, A131
Yurchenko S. N., Mellor T. M., Freedman R. S., Tennyson J., 2020, MNRAS, 496, 5282

ORIGINAL UNEDITED MANUSCRIPT

Downloaded from https://academic.oup.com/mnras/advance-article/doi/10.1093/mnras/stae1110/7657811 by guest on 28 April 2024